Microfabricated Differential Reactor for Heterogeneous Gas Phase Catalyst Testing

Sameer K. Ajmera, Cyril Delattre, Martin A. Schmidt,* and Klavs F. Jensen[1]

*Department of Chemical Engineering and *Microsystems Technology Laboratories, Department of Electrical Engineering and Computer Science,
Massachusetts Institute of Technology, 77 Massachusetts Avenue, Cambridge, Massachusetts 02139*

A differential packed-bed reactor microfabricated in silicon is presented for heterogeneous gas phase catalyst testing. A novel cross-flow design achieves uniform flow distribution over a wide (25.5 mm) but shallow (400 μm long × 500 μm deep) catalyst bed to realize differential conversions with sufficient reaction to allow monitoring with conventional analysis techniques. The use of catalyst particles (diameters 53–71 μm) implies that conventional synthesis procedures can be used and experimental results translated to catalysts in macroscopic reactors. A set of shallow microfabricated channels maintains a spatially uniform pressure drop irrespective of variations in catalyst packing. Experiments and finite element simulations confirm the bed is isobaric with even distribution of flow. Quantitative analysis of transport effects indicates the microreactor also suppresses thermal and mass gradients in the catalyst bed. These characteristics make the cross-flow microreactor a useful tool for experiments to obtain kinetics and optimize reaction conditions. Experiments with CO oxidation confirm the ability of the microreactor to obtain kinetic and mechanistic information that compare well with parameters previously determined in macroscale systems. Reactor modeling also indicates that the catalyst bed operates differentially even at total conversions that would be considered large in traditional plug flow reactors, adding to the utility of the cross-flow microreactor as a laboratory tool.   © 2002 Elsevier Science (USA)

Key Words: microreactor; microchemical; microfabrication; catalyst testing; screening; high throughput; kinetics; CO oxidation; cross-flow.

INTRODUCTION

Interest in faster development of new catalysts has driven advances in high-throughput screening, in particular combinatorial methods and novel characterization techniques (1–8). With the ability to rapidly screen for promising leads among a large number of catalyst samples comes the need for further characterization of these promising candidates for optimal operating regimes, kinetics, and lifetime and for translation into actual reactor environments. Microfabrication of chemical reactors provides unique opportuni-

ties for parallel, efficient testing of catalysts (9). Reducing reactor size reduces concentration and thermal gradients, which otherwise would confound kinetic data. Microfabrication also gives flexible control over reactor geometry and design, enabling flow manifolds and reactor configurations that are difficult to realize in macroscopic testing systems. Moreover, incorporation of sensors and actuators as in microchemical analytic devices, "micro-total-analysis-systems" (μTAS) (10), could ultimately result in integrated testing platforms as replacements for individual feed conditioning systems, reactors, and analytical instruments (11). Catalysts in the powdered or particle form mirror those used in large-scale reactors and thus ease the transfer of results from miniaturized catalyst testing platforms to industrial processes.

Heterogeneous gas phase catalyst testing is often performed on the bench-scale in mini tube reactors approximately 5 mm in diameter with catalyst particles packed against a glass frit. Even at this scale, the reactors are susceptible to thermal and concentration gradients that negatively impact the speed and accuracy of kinetics measurements. Tube reactors have axial or tube flow (i.e., flow along the longitudinal axis of the tube). A microfabricated packed-bed reactor based on an axial flow design with ~60 μm catalyst particles has demonstrated the potential of using microfabricated reactors to obtain chemical kinetics (12, 13). Although the reduced reactor length scale helped suppress thermal and concentration gradients, the pressure drop along the micro packed-bed increased significantly due to the small catalyst particle size. Gas flow rates as low as 4.5 sccm through the 20-mm-long bed yielded a pressure drop as large as 0.4 atm (13). Since pressure drop in a packed bed is roughly inversely proportional to the square of the particle diameter, a micro packed bed with 60-μm catalyst particles has ~275× larger pressure drop than a bed with 1-mm particles, and ~27500× larger pressure drop than a bed with 10 mm particles (for a given bed length). It is often desirable, particularly with unknown kinetic mechanisms, to run a catalyst testing reactor differentially (low reactant conversions), which can be achieved by using larger reactant flow rates. However, larger flow rates

---

serve to further increase the already large pressure drop in microfabricated reactors. Using less catalyst by reducing the bed length would lower conversions and decrease the pressure drop. However, it is desirable to have as much catalyst as possible in microfabricated reactors to allow measurable reactant conversions while still maintaining practical flow rates, particularly for slow reactions. A larger quantity of catalyst also affords an increased flow rate that reduces lag time in testing systems and helps average out variances in catalytic properties between particles. In general, for microfabricated chemical systems, it is desirable to have as much catalyst as possible, but it is necessary to shorten the length of the catalyst bed to reduce pressure drop.

In this work, we introduce a silicon differential packed-bed microreactor for catalyst testing that uses standard catalyst particles and a novel cross-flow design. The cross-flow geometry enables the use of practical flow rates and catalyst quantities while minimizing pressure drop. Pressure drop studies and flow simulations were performed to characterize the performance of the microreactor. Kinetic experiments with the microreactor are presented to demonstrate the utility of the microfabricated cross-flow reactor as a practical laboratory research tool. Finally, quantitative analysis and reactor modeling are described to better understand the benefits of the small reactor length scale and cross-flow geometry for suppressing gradients as well as expanding the window of operation for differential reactor behavior.

THE CROSS-FLOW MICROREACTOR

The cross-flow design integrates short parallel packed beds into a continuous wide bed (Fig. 1), reducing pressure drop while maintaining catalytic area. The shorter bed length and decreased superficial velocity due to the increased cross-sectional area reduce the pressure drop through the reactor. Figure 2 details the silicon microfabricated cross-flow reactor. The reactor has one inlet and one out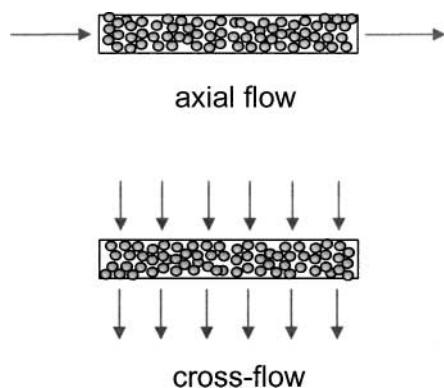let for gas flow. The inlet channels bifurcate into 64 parallel channels that feed a wide catalyst bed (Figs. 2a, 2b). The catalyst bed is 25.55 mm wide, 500 μm deep, and 400 μm long and is approximately 5.1 μl in total volume. An array of catalyst retainer posts (50 μm wide) acts as a filter to hold the bed in place (Fig. 2c). The heads of the retainer posts expand out to leave a 35–40 μm gap between posts, setting the lower limit for particle size. A designed pressure drop created by 256 shallow channels maintains even flow distribution across the wide bed (Fig. 2d). The channels are 40 μm wide and 20–25 μm deep and meander for 1.265 mm in length (net centerline length = 2.165 mm). The pressure drop through these channels is intentionally greater than the pressure drop through the rest of the reactor, including the catalyst bed. Consequently, variances in catalyst packing density minimally influence the pressure drop through the reactor and negligibly impact the overall flow distribution. The tight dimensional control and reproducibility of the pressure drop channels achievable with microfabrication technology insures the uniformity of flow throughout the reactor. The reactor contains three different channel depths. The pressure drop channels are ∼20 μm deep, while the inlet and exit flow manifold is etched 370 μm deep. The packed-bed region is 500 μm deep (a single silicon wafer thickness). Figure 2e shows a cross-section schematic detailing the relative depths of these microchannels. Along the perimeter of the microreactor are four side-wells to insert thermocouples. The large thermal conductivity of single crystal silicon (150 W/(m · K)) and the high surface to volume ratio imply that the packed bed quickly achieves thermal equilibrium with the bulk reactor.

The cross-flow microreactor is similar to a bench-scale reactor for catalyst testing that uses a shallow bed with only a few layers of catalyst particles to achieve differential operation. However, these reactors have difficulty ensuring even distribution of reactants across the wide bed because variations in packing density (voids) and nonuniformities in the glass frit significantly impact the pressure drop through the reactor. These variations lead to channeling and bypassing of catalyst particles as fluids preferentially take paths of lower pressure drop. The integration of the microfabricated pressure drop channels and bifurcated inlets eliminates these concerns in the cross-flow microreactor. Heat transfer into and out of the catalyst bed is also enhanced in the cross-flow geometry over bench-scale shallow packed-beds. In the microreactor, heat transfer along the shortest bed dimensions (500 μm height and 400 μm length) is the primary mode of heat removal. In addition, most of the reactor wall area in contact with the particles lies along this primary mode of heat transfer. In contrast, in a bench-scale shallow packed-bed, radial heat transfer to the sidewalls (the largest bed dimension) is the primary mode of thermal transport out of the packed bed and only a small fraction of the reactor wall area in contact with the catalyst particles lies along this direction.
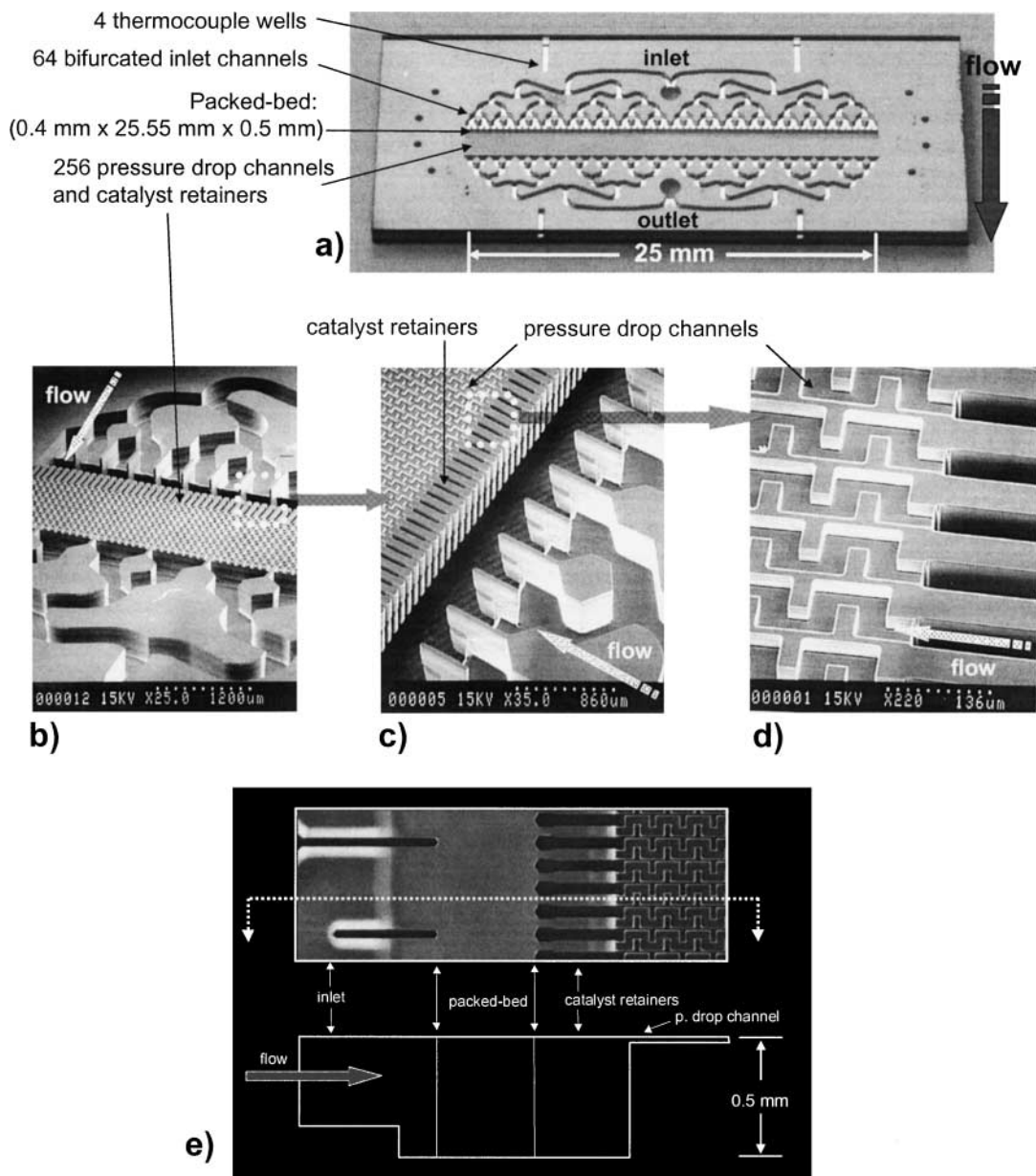

FIG. 1. The cross-flow design: short parallel packed beds are integrated into one continuous wide bed with flow along the short axis.

FIG. 2. The microfabricated silicon cross-flow reactor. (a) Photograph of the silicon microreactor chip. (b–d) Scanning electron micrographs of the microreactor at different magnifications. The reactants are bifurcated into 64 inlets that feed a shallow catalyst bed. Catalyst retainers keep the bed in place while shallow pressure drop channels maintain even flow distribution across the bed. (e) A photograph of the packed-bed region of the microreactor and an accompanying cross-section detailing the relative depths of the microchannels.

Catalyst is loaded into the reactor through the inlet port using a vacuum placed at the outlet. The flow of gas generated by the vacuum is enough to fluidize the small catalyst particles and draw them into the reactor. Figure 3 shows a photograph of a microreactor packed with 60-μm glass beads. Clogging or plugging in the curved inlet channels does not occur during loading. The pressure drop channels are placed after the packed-bed to allow the catalyst to be packed through the inlet, eliminating the need for separate catalyst loading ports that would contribute dead

volume to the reactor. The microreactor is reusable as catalyst can be recovered by applying a high pressure to the outlet and blowing the particles out of the inlet port. The particles can be captured on a filter for post-reaction analysis if desired.

The microreactor is fabricated out of single crystal silicon with standard microfabrication processes (14, 15) developed for integrated circuits and MEMS (MicroElectroMechanical Systems). Geometry is defined using photolithography and created with silicon etching. The inlet and outlet
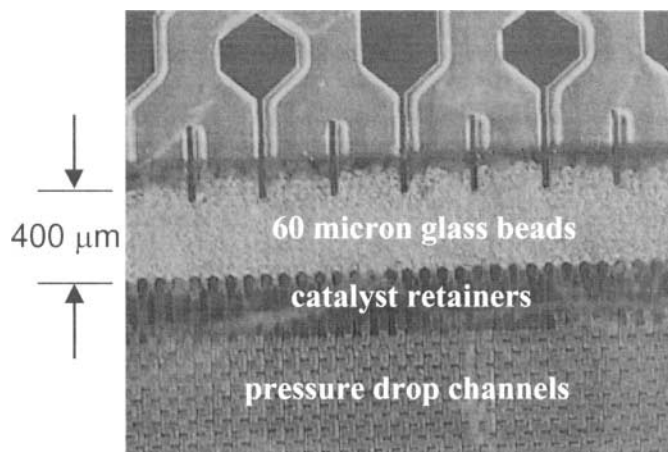
FIG. 3. Photograph of a microreactor packed with glass beads.

ports, flow channels, and thermocouple wells are etched into a silicon substrate (100 mm diameter wafer, 500 μm thick) using multiple time-multiplexed inductively coupled plasma etches (16). The channels are capped on the top and bottom with Pyrex wafers (Corning 7740), which have a thermal coefficient of expansion similar to that of silicon, using an anodic bond (17). The bottom Pyrex wafer has 2-mm mechanically drilled holes that are aligned to the inlet/outlet ports during the bonding process. The bonded wafer stack is cut with a die saw to obtain individual reactor chips. A 100-mm-diameter wafer yields eight cross-flow reactors (15 mm × 40 mm × 1.5 mm) after bonding and dicing. The annealing point of Pyrex sets the maximum operating temperature of the device at ~775 K, which covers a broad range of heterogeneous processes. If higher temperatures are desired, silicon capping wafers can be used instead of Pyrex, raising the operating limit to above 1275 K. For initial microreactor characterization, Pyrex offers the

advantage of being optically transparent. Other technologies such as ceramic molding or the lamination of thin layers of ceramics or intermetallics are under development to achieve microstructures for high-temperature operation (18–20). However, silicon offers better dimensional control and the advantages of highly parallel and reproducible manufacturing.

EXPERIMENTAL

After fabrication, the microreactor is integrated into a catalyst testing station (Fig. 4). The reactor is compressed with a metal cover plate against a thin elastomer gasket (0.8 mm Kalrez or Viton) with punched through-holes to form fluidic connections to a stainless-steel base in a fashion similar to that described by Losey *et al.* (12). External fluidic connections are made directly to the metal base. The metal compression plate and the base contain cartridge heaters and thermocouples that are inserted into the side-wells of the reactor. Temperature control is achieved using a standard temperature controller. The microreactor assembly is connected to the rest of the system via standard fittings, valves, and 1.6-mm-O.D. stainless-steel tubing. Mass-flow controllers are used to control gas flow. The entire system is placed inside a small ventilated enclosure similar to a standard chemical fume hood. This highlights an inherent benefit of working with microreactors as tube furnaces, sand baths, and other structures that add size and complexity to typical laboratory work are not needed. Multiple reactors can be run side-by-side with minimal increase in system size.

Pressure drop experiments with nitrogen gas flow were carried out using Grade A (ASME) pressure gauges and 60-μm glass beads (MO-Science Inc.) as packing. 2-D modeling of gas flow in the reactor to examine flow distribution across the reactor depth and the effects of diffusion was done using a commercial finite element software package (FEMLAB, COMSOL Inc.) on a PC platform.
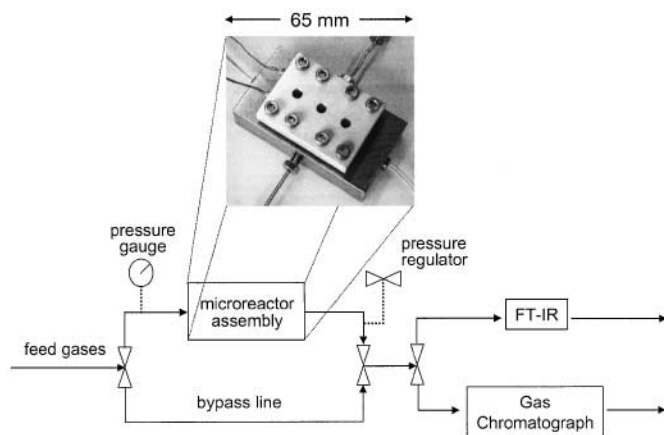

FIG. 4. Catalyst testing setup: The reactor is compressed against a gasket with an aluminum top plate to form fluidic connections to a stainless-steel base that is integrated into a catalyst test station.
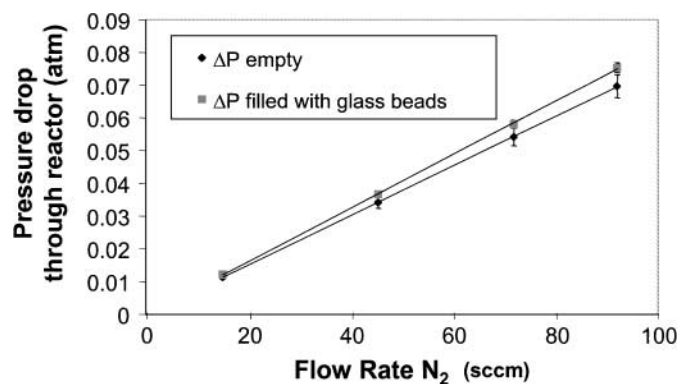

FIG. 5. Pressure drop across an empty reactor (lower curve) and one packed with 60-μm glass beads (upper curve). The addition of packing has a small affect on the total pressure drop (~7%), minimizing the effect of variances in packing density on the overall flow distribution.
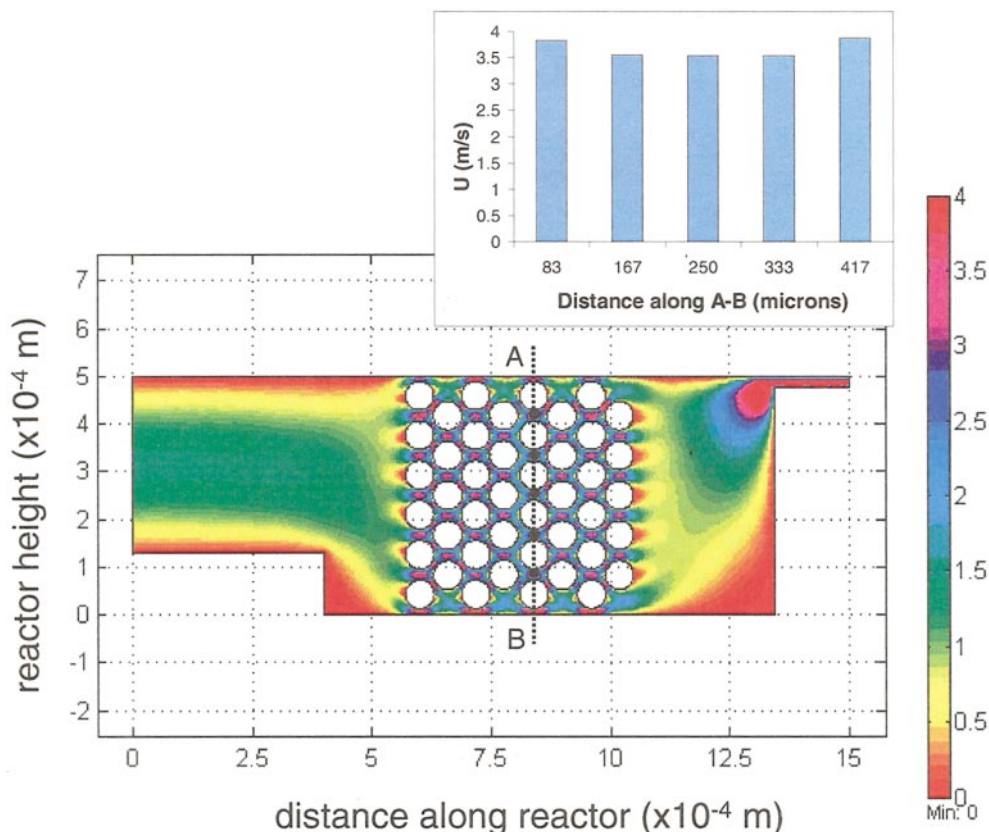
FIG. 6. 2-D finite element model showing the velocity profile (m/s) through a reactor cross-section packed with 60-μm "particles" with air flow at 1 m/s and 373 K. The particles serve to flatten the parabolic laminar profile that would occur in an empty reactor. The velocities shown in the graph correspond to the peak velocities in the space between the particles represented by the black dots.

The oxidation of carbon monoxide over supported metal catalysts was performed as a model reaction. Chemical detection was performed by either a micro gas chromatograph with a thermal conductivity detector and a Mol Sieve 5-Å column (Agilent Technologies) or an FT-IR spectrometer (Analect) with a 100-cm^3 gas cell. The microreactor was loaded with approximately 3 mg of alumina-supported metal catalyst (1 wt.% Rh, Pt-Alpha Aesar, 0.3 wt.% Pd-Institut Français du Pétrole) sieved between 53–71 μm and loaded with a vacuum in air. Available metal surface area for the rhodium and platinum catalysts was estimated using CO adsorption at 313.15 K (Micromeritics Instrument Co.) and found to have dispersions of 2.9% and 23% respectively. The palladium catalyst was reported by the supplier to have 35% metal dispersion. The reactor was run vertically with downward flow in order to prevent fluidization of the particles. A back pressure regulator was placed after the reactor assembly to maintain constant reactor pressure.

Before each experimental run, the catalyst was pretreated *in situ* at 523 K for 1 h with oxygen flow followed by 1 h under hydrogen. A premixed tank of high purity 1%CO/1%O$_2$ in helium (BOC Gases) at flow rates between 20 and 600 sccm was used for the reactant feed. Reaction order experiments were performed by blending the premixed feed with a second 1%CO or 1%O$_2$ in He mixture in the appropriate quantities. All experimental kinetics reported with the microreactor were performed in the differential regime for steady-state CO conversions of $\sim$10% or less.
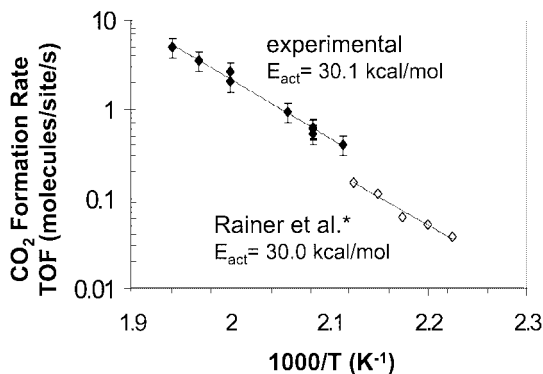

FIG. 7. Experimental turnover frequency (TOF) for CO oxidation over 0.3 wt.% Pd/Al$_2$O$_3$ with 1%CO/1%O$_2$ feed. The results agree well with those of *Rainer et al.* (24) taken for CO oxidation over 0.1 wt.% Pd/Al$_2$O$_3$. The data published by Rainer et al. were originally taken with a 0.58%CO/0.3%O$_2$ feed and have been scaled to 1% in this figure using their published reaction orders.

Steady state was typically obtained in under a minute. Temperatures up to 546 K were used and the reactor assembly was heated without external cooling. The absolute pressure at the exit of the reactor was nominally atmospheric. The inlet pressure and the pressure drop across the catalyst bed are discussed in the following section.

RESULTS AND DISCUSSION

Pressure Drop Channels

The pressure drop across the reactor was measured for both an empty reactor and one packed with glass beads (Fig. 5). The pressure drop across the empty reactor was approximately 0.075 atm (1.1 psi) for 100 sccm nitrogen flow at room temperature. The addition of packing only contributed ~7% to the total pressure drop with majority of the drop created by the shallow pressure drop channels. This implies that in the worst case where a large portion of the reactor could be entirely void of catalyst (unlikely in normal operation), flow rates between this region and the rest of the reactor would vary by only ~7%. In normal operation with a relatively even distribution of packing, flow through the reactor is independent of the catalyst particles, and the pressure drop across the packing is very small. At 100 sccm gas flow, the drop across the bed was only 0.006 atm (0.08 psi). The bed can be considered isobaric at these flow rates (typical in normal operation), eliminating a complication in kinetic analysis. The benefit of the cross-flow design is seen when compared to the pressure drop of the same reactor geometry in axial (tube) flow. Using the Ergun equation (21), the pressure drop in an axial flow reactor of the same geometry and glass packing would be ~1600 × larger for 100 sccm gas flow. The low pressure drop and even flow distribution obtained in the cross-flow design are clear advantages for obtaining accurate kinetics.

Flow Distribution—Modeling

2-D finite element flow calculations were performed using the reactor cross-section shown in Fig. 2e as a computationally feasible means of understanding flow distribution across the depth of the reactor. The calculations were done using air flow at an average velocity of 1 m/s at 373 K for a reactor filled with eight layers of 2-D circular "particles." The 2-D model is a reasonable approximation of the flow across the reactor cross section as the width of the particle bed is approximately 60 times the length. The convective velocity field was calculated for the entire reactor cross-section and the velocity profile at a particular section is shown in Fig. 6. The parabolic velocity profile that would be seen in an empty reactor is replaced by an even distribution of fluid across the reactor depth. The velocity profile for Section A–B shows that the peak velocities between particles (indicated by the black dots in Fig. 6) are slightly higher at the wall because of the higher porosity. This effect is diminished with increasing particle loading. The sizes of the recirculation zones are on the order of a single particle and are not directly inside the packed-bed region. The characteristic diffusion time for a gas across a 60-μm length is less than 0.02 ms, while the residence time in the packed-bed is approximately 0.4 ms. At this length scale, diffusion is very fast and counters the trapping effects of any stagnant volume. Therefore, a microreactor packed with actual spherical catalyst particles will have an even distribution of flow across the entire reactor depth with minimal effects from recirculation zones, rendering a device useful for kinetics studies.

Oxidation of Carbon Monoxide

To validate the cross-flow microreactor as a tool for obtaining chemical kinetics, turnover frequency (TOF, molecules of product formed per catalyst site per second), apparent activation energy, and reaction orders for CO oxidation were determined experimentally. CO oxidation was chosen because it is a well-studied reaction and the observed kinetics are well understood, particularly in the "CO inhibiting regime" in which the microreactor experiments were performed (22). For conditions where the CO/O_2 concentration ratio is greater than ~0.08, CO oxidation occurs in the CO inhibiting regime with CO dominating the surface coverage of the catalyst due to its large sticking coefficient (22, 23). In this regime, the reaction rate is governed by the desorption rate of CO from the catalyst surface and therefore is approximately positive first order in O_2 concentration and negative first order in CO concentration. CO oxidation on Pd, Rh, and Pt supported on alumina catalysts has been found to be structure insensitive at atmospheric pressures and near stoichiometric feeds (22, 24, 25), although Zafiris and Gorte (26) have reported some evidence of structure sensitivity for Pt.

As expected, no temperature increase was detected upon switching flow from the bypass line to the reactor due to the ability of silicon to readily dissipate heat. The thermal mass of the stainless steel packaging is also many orders of magnitude larger than that of the reactor and provides a significant heat sink. Likewise, the energy provided by the cartridge heaters to maintain the temperature of the reactor/packaging is significantly larger than the energy generated from the heat of reaction. This gives fine temperature control over the exothermic reaction. The pressure drop in the packed-bed ranged between 0.002 and 0.15 atm depending on the flow rate and is considered constant for kinetic analysis. The reactor pressure was adjusted between 1.0 and 2.5 atm and was controlled by the pressure regulator. The Reynolds number based on catalyst particle diameter ranged from 0.0051 to 0.153.

Figure 7 shows the experimental TOF for the 0.3 wt.% Pd/Al_2O_3 catalyst with $1\%CO/1\%O_2$ reactant feed at 1.3 atm compared to previously published values by Rainer

TABLE 1

Apparent Activation Energy for CO Oxidation over Different Catalysts in the Microreactor Compared to Literature Values

Catalyst	Microreactor E_{act} (kcal/mol)	Literature E_{act} (kcal/mol)	Literature reference
0.3 wt.% Pd/Al$_2$O$_3$	30.1	30.0	(24)
1 wt.% Pt/Al$_2$O$_3$	20.0	21.6	(27)
1 wt.% Rh/Al$_2$O$_3$	27.6	24–31	(25, 28)

et al. for 0.1 wt.% Pd/Al$_2$O$_3$ (24). The original results by Rainer *et al.* were obtained for a 0.58% CO and 0.3% O$_2$ feed at atmospheric pressure. For proper comparison to our reaction conditions, their data shown in Fig. 7 were scaled appropriately to 1% using reaction orders of −0.78 for CO and +0.84 for O$_2$ as published. Both the TOF and the apparent activation energy (30.1 kcal/mol) agree well with the previously reported values. Similar agreement with literature was also seen for the 1 wt.% Pt/Al$_2$O$_3$ and 1 wt.% Rh/Al$_2$O$_3$ catalysts, showing the ability to accurately distinguish the performance of different catalyst samples. Table 1 summarizes the activation energies obtained with the microreactor for the various catalysts compared with published values (24, 25, 27, 28) determined under reaction conditions similar to the microreactor experiments. Figure 8 shows the dependence of TOF on both CO and O$_2$ partial pressures at 505 and 540 K with the 1 wt.% Pt/Al$_2$O$_3$ catalyst. The experimental reaction orders of −0.79 for CO and +1.0 to +1.5 for O$_2$ agree with the respective orders of −0.6 ± 0.3 and +1.3 ± 0.3 obtained by Zafiris and Gorte (26) at 650 K and clearly show the positive dependence on O$_2$ and the negative dependence on CO predicted by the proposed reaction mechanisms. The ability to obtain mechanistic information such as reaction order is important to fully characterize and understand a catalytic process and is often the most difficult type of information to obtain in high-throughput reactor systems. The consistency of the data with different catalysts and the ability to extract specific kinetic information such as reaction order illustrates the potential of the cross-flow microreactor as a robust tool for catalyst testing.

Examination of Transport Limitations

To quantitatively understand the advantages of the microreactor, it is necessary to examine different transport phenomena in the microreactor under reaction conditions using representative criteria. The Weisz modulus, Mw, gives an indication of the internal diffusion limitation within a catalyst particle (29);

$$M_w = \frac{R_{rxn} r_p^2}{D_e C_s}. \quad [1]$$

Using the fastest reaction rate observed (TOF ∼ 10), an estimated bed void fraction of 0.40, a typical particle void fraction of 0.5, and an estimated upper bound on particle tortuosity of 7.5, Mw is approximately 0.01. The small Weisz modulus indicates the catalyst particles are small enough to prevent concentration gradients from forming internally. Anderson (30) proposed a criterion for assuring that the observed reaction rate does not differ from the actual reaction rate within a catalyst particle by more than 5% due to intraparticle temperature gradients:

$$\frac{|\Delta H| R_{rxn} r_p^2 E_{act}}{k_p T_s (RT)} < 0.75. \quad [2]$$

The catalyst particles may be considered isothermal as the left hand side of the inequality is ∼0.01 using experimental data and an estimate of 0.1 W/(m · K) for the thermal conductivity of porous alumina. In both criteria above (Eqs. [1] and [2]), mass and heat transport are inversely related to the square of particle size. The small particles used in the microreactor eliminate internal transport limitations.

External transport effects are more difficult to estimate due to the lack of literature data for heat and mass transfer coefficients at low Peclet numbers. Correlations for the Sherwood and Nusselt numbers at low Peclet numbers are not well understood in the flow regimes seen in the microreactor and their applicability is unclear (31, 32). The reactor Peclet number, Pe$_r$, ranges between 0.1 and 1.0 for the oxidation experiments. At these flow rates, diffusion plays a significant role in mixing and transport in the reactor and dominates over convection at the lower range of flow rates. In the limiting case of mass transfer, where Reynolds number approaches zero, diffusion is the only form of transport to the catalyst surface. An order of magnitude analysis of the transport around a catalyst particle can be made by examining the gradients needed to maintain the flux of molecules and energy corresponding to the reaction rates observed in the oxidation experiments. Since the kinetic data were taken differentially, the flux of reactants to each particle is approximately the same. Assuming a worst case scenario where the center of each particle is two particle diameters away from its closest neighbor (i.e., a "shell" with a radius of a particle diameter surrounds each particle), a Fick's law analysis shows that the concentration gradient across this shell is approximately 0.015% of the bulk reactant concentration. For 1% CO at 1.3 atm total pressure, the concentration on the catalyst surface differs from the bulk by only 5×10^{-5} mol/m^3 and this difference is negligible compared to the bulk concentration of 0.3 mol/m^3. Furthermore, interstitial diffusion time from one particle to another (taken as 1 particle diameter) is on the same order as the residence time across a single particle; i.e., Pe$_{particle}$ ∼ 1. Therefore, mass transfer to the catalyst surface is not limiting and the reactant concentrations may be taken as the bulk.
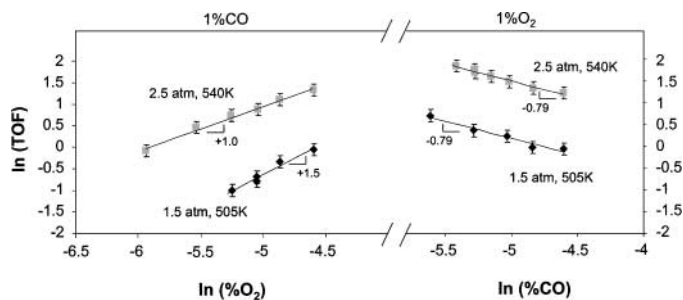
FIG. 8. Reaction order for O_2 and CO at 505 and 540 K for CO oxidation over 1 wt.% Pt/Al_2O_3 obtained at differential conversions. The negative order of CO and positive order of O_2 expected from proposed reaction mechanisms are clearly observed.

An analogous calculation to Fick's law for the thermal gradient necessary to completely remove the heat generated by reaction from the particle can be made. Similarly, for differential conversions, the heat generated by each particle is approximately the same. For the oxidation reactions, the temperature at the catalyst surface is calculated to differ by only ~0.01 K from the surrounding fluid (taken 1 particle diameter away from the particle center), yielding no external temperature gradients. Table 2 summarizes the calculations of transport properties in the microreactor and shows that the small length scale obtainable in microfabricated reactors serves to avoid gradients that would otherwise complicate kinetic analysis. Even though CO oxidation is a relatively simple chemistry, the reduction of gradients indicated by the calculations would carry over to more complicated reaction systems, facilitating the extraction of useful information from the microreactor.

Characterization of the Cross-Flow Geometry—Diffusional Mixing

The small reactor dimensions and short bed length relative to the flow direction create mixing characteristics on the reactor scale different from those of a typical axial flow microreactor. In previous axial flow micro packed beds, reactor Peclet numbers up to 360 were achieved for gas flow

rates as low as 8 sccm, assuming the plug-flow reactor (PFR) assumption to be valid (13). In contrast, the small reactor Peclet numbers (0.1–1.0) in the cross-flow design for flow rates as large as 600 sccm indicate that axial diffusion is extremely important and the reactor deviates significantly from plug-flow. The residence time across the cross-flow catalyst bed varied between 0.6 and 8.0 ms for the CO oxidation experiments. In comparison, the characteristic time of diffusion across the 400 μm length of the packed-bed (assuming an empty reactor) is approximately 0.8 ms, and is within the same order as the bed residence time. Therefore, diffusion significantly affects the concentration profile along the microreactor, and hence, the reactor performance.

In order to better understand the effect of diffusion on the concentration profiles in the reactor, a 2-D reaction–diffusion–convection finite element model using the same cross-section shown in Fig. 6 was examined for CO oxidation at various reactant conversions. In order to simulate the effect of the bifurcated inlets, the inlet section in Fig. 6 was extended upstream to include channels of appropriate length with decreasing cross-sectional area. This way, the increased convective velocity in each subsequent upstream bifurcation is captured and the extent to which back diffusion affects the concentration of reactants before the packed bed can be assessed. Both convective momentum (Navier–Stokes) and mass balances with reaction terms (21) were used in the calculations and the heterogeneous reaction was confined entirely to the surface of each catalyst particle. A Langmuir–Hinshelwood mechanism for CO oxidation (27) was used to describe the reaction kinetics:

$$R = \frac{k \cdot C_{CO} \cdot C_{O_2}}{(1 + K \cdot C_{CO})^2}. \qquad [3]$$

It has been shown that the reaction operates in the "CO inhibiting regime" at large CO concentrations, reducing Eq. [3] to

$$R = \frac{k_1 \cdot C_{O_2}}{C_{CO}}, \qquad [4]$$

where $k_1 = k/K^2$ is the observable rate constant obtained from kinetic experiments. Equation [4] describes the observed positive order in oxygen and negative order in CO. Oscillatory behavior corresponding to changes in the catalyst surface coverage has been reported at P_{O_2}/P_{CO} ratios higher than 25 for CO oxidation on Pt at atmospheric pressures (33). This concentration ratio is approached at CO conversions of 98% or higher for the 1% CO, 1% O_2 feed used in our oxidation experiments. Therefore, flow rates for the simulations were chosen to give total conversions much lower than 98% to maintain the validity of using the mechanism represented by Eq. [4].

TABLE 2

Summary of Calculations of Transport Limitations in the Microreactor for CO Oxidation

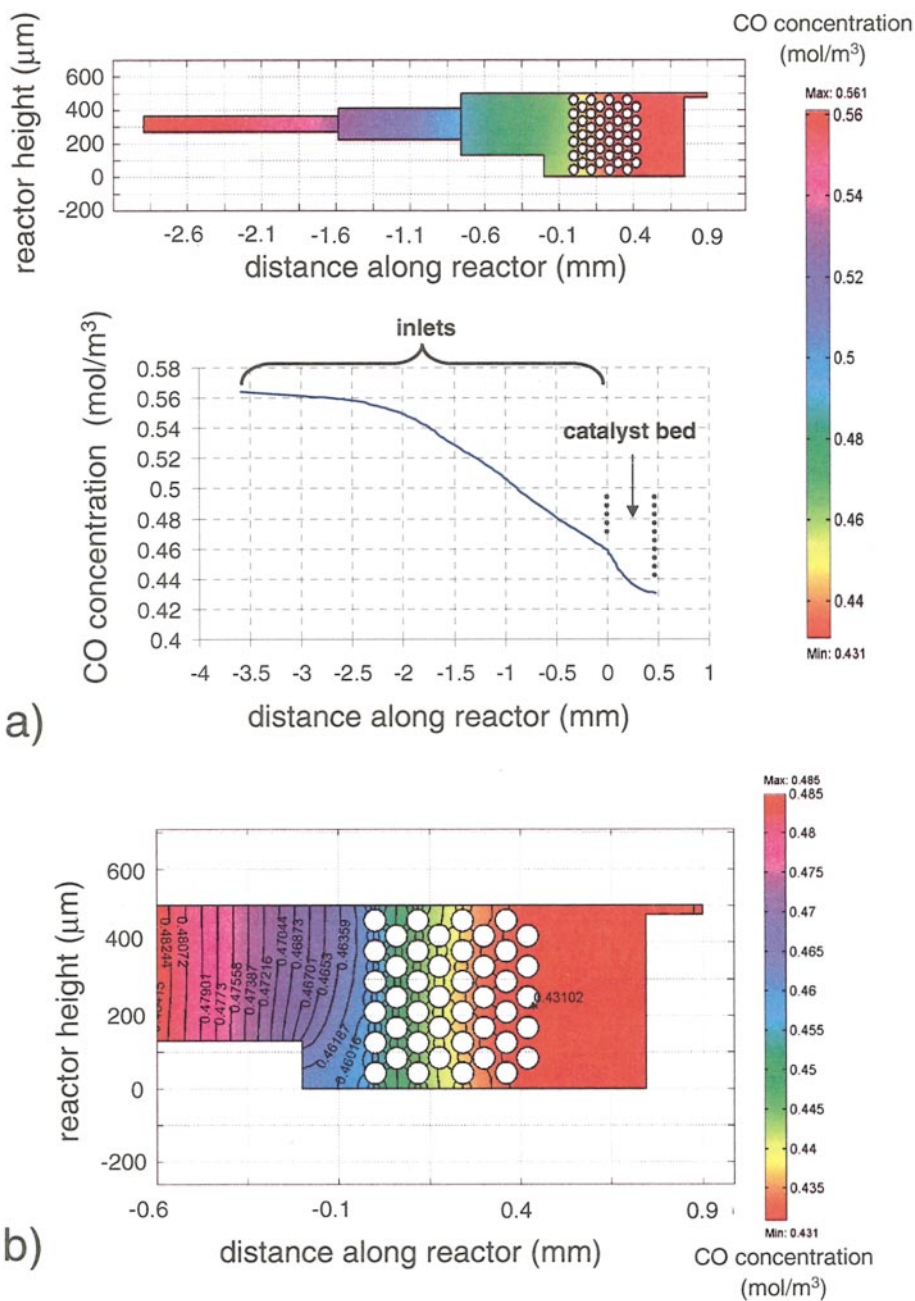|	Criterion	Estimation	Not transport limited if
Internal	Mass (M_W)	0.01	$\ll 1$
	Thermal (Anderson)	0.01	<0.75
External	Mass	$\Delta C = 0.015\%$	Close to 0
(diffusion only)	Thermal	$\Delta T = 0.002\%$	Close to 0

FIG. 9. Finite element models of the CO concentration profile in the cross-flow microreactor for CO oxidation at 540 K, 2.5 atm, and an inlet concentration of CO of 0.564 mol/m³. (a) Profile along the reactor including 2.75 mm of upstream inlet channels. The decreasing cross-sectional areas indicate points of bifurcation and capture the corresponding increases in convective velocity. (b) Close-up view of the CO concentration profile across the catalyst bed.

Figure 9a shows the concentration profile for the reactor with approximately 2.75 mm of inlet channels extending upstream from the packed bed. Each cross-section reduction represents a point of bifurcation. The calculations were performed for CO oxidation at 540 K with a feed velocity corresponding to 97 sccm and inlet CO and O_2 concentrations of 0.564 mol/m^3 (corresponding to 1% CO and 1% O_2 at 2.5 atm pressure as performed experimentally). The kinetic rate constant, k_1, was chosen to yield the same level of conversion observed in microreactor experiments under the same reaction conditions. A conversion of 24% is seen for the model. Although the reaction only occurs in the catalyst bed, the CO concentration falls over the entire 2.5 mm of inlet channels shown in the figure due to diffusion effects. Axial diffusion implies that the CO concentration decreases well before the beginning of the catalyst bed, showing that the reactor operates in a regime significantly deviating from a PFR. The behavior is similar to the classical dispersion models between a PFR and a continuous-stirred tank reactor (CSTR), with a small Pe lying closer to the CSTR limit. An added benefit of the bifurcated inlet design is seen as the increased upstream convective flow velocities serve to impede the penetration of back diffusion. With over 17.5 mm of inlet channels in the reactor, the 2.75 mm penetration depth seen in Fig. 9 is small enough that all back diffusion is confined to the microreactor and will not affect system components upstream of the reactor. Figure 9b shows the catalyst region in more detail. The concentration at the beginning of the packed-bed of ~0.46 mol/m^3 corresponds to a conversion of ~18.4% even though no reaction occurs in the inlet channels. In fact, the concentration in the catalyst bed itself varies only by ~6%, indicating that even at large total conversions (24%, as in the present case), the bed still operates close to differentially. This behavior allows kinetic measurements to be obtained at what would have been large conversions in a traditional reactor and thus expands the utility of the cross-flow reactor for catalyst testing.

The calculations shown in Fig. 9 were repeated for various reaction rate constants while keeping flow rate constant to simulate reactor performance at different levels of conversion. Table 3 summarizes these results. It is seen that for conversions as high as 34%, the concentration across the catalyst varies by less than 10% consistent with the interpretation that the reactor approximates a CSTR. With the given reactor conditions, differential kinetics (previously defined as conversions less than 10%) can be obtained even at these traditionally large conversions. If tighter limits on reactant conversion are desired to characterize differential operation (e.g., <2%), the microreactor behavior scales accordingly. A conventional bench-scale shallow bed reactor, when packed with a few layers of particles of similar size as the microreactor, also has the capability of achieving the

TABLE 3

Summary of Convection–Diffusion–Reaction Calculations at Varying Reaction Rates

Kinetic rate constant $(k_1)^a$	CO conc. at front of catalyst bed (mol/m^3)	CO conc. at end of catalyst bed (mol/m^3)	Total CO conversion in reactor	Variation of CO across catalyst bed
$0.6k_1$	0.51	0.49	12%	3.9%
k_1	0.46	0.43	24%	6.5%
$1.3k_1$	0.42	0.38	34%	9.5%
$1.6k_1$	0.36	0.31	45%	13.9%

Note. $T = 540$ K; CO feed concentration $= 0.564$ mol/m^3; total feed rate $= 97$ sccm; feed $= 1\%$CO/$1\%O_2$ in He.

^{a} k_1 is based upon the level of conversion observed in the microreactor CO oxidation experiments under the same conditions.

low Peclet numbers needed to expand the range of conversion for which the differential reactor assumption is applicable. However, difficulties arise in insuring the catalyst is evenly distributed across the reactor cross-section with uniform depth. Further, the use of larger particles increases the reactor Peclet number and diminishes the beneficial effects of back diffusion in the reactor. The small length scales achievable in the microreactor and the management of flow geometry and catalyst bed dimensions serve to controllably expand the window of operation for differential catalyst testing, adding flexibility and efficiency over many current catalyst testing platforms.

CONCLUSIONS

A microfabricated silicon cross-flow microreactor for differential heterogeneous gas phase catalyst testing has been presented. The microreactor uses high-surface-area porous catalyst particles synthesized by standard procedures. By employing catalyst particles instead of thin-films or coatings, current industrial catalysts and preparation methods from a wide range of applications can be tested, and relevant kinetic parameters can be determined quantitatively. Unlike axial flow microreactor designs that are susceptible to large pressure drops, the cross-flow design yields an isobaric catalyst bed that utilizes practical quantities of catalyst and flow rates. The consistency of kinetic parameters (turnover frequency and activation energy) and mechanistic information (reaction order) obtained in the microreactor with previously reported values across different catalysts demonstrates the potential of microfabricated cross-flow reactors as laboratory tools for heterogeneous catalyst testing. A quantitative analysis of the transport effects in the microreactor indicates that the small catalyst particle size and reactor geometry eliminate mass and thermal gradients both internal and external to the catalyst

particles. By reducing thermal, mass, and pressure gradients and ensuring even flow distribution over the catalyst bed, the cross-flow microreactor provides a useful platform for the determination of kinetic parameters. Reactor simulations demonstrate that the reactor performance is consistent with a small Pe number dispersion model approaching CSTR behavior (Pe → 0). The models suggest the cross-flow geometry enables differential operation across the catalyst bed at what would be large total conversions in traditional plug flow reactors. This increased window of operation is advantageous for greater efficiency and robustness in catalyst testing and suggests the cross-flow geometry could serve as basis for the development of microfabricated packed-bed reactors that operate as CSTRs. Because the cross-flow microreactor was designed to be a fully functional chemical reactor utilizing catalyst particles, the reduction of gradients, expanded window of operation, low pressure drop, and even flow distribution are advantages that apply to chemistries more complicated than CO oxidation, facilitating the extraction of useful information during catalytic studies. The microfabrication approach to reactor development also has the potential for integrating several catalyst testing microreactors together into a high-throughput catalyst testing platform to accelerate both catalyst discovery and optimization while providing relevant quantitative kinetic information on standard porous supported catalyst particles.

APPENDIX: NOMENCLATURE

C_s	Concentration of limiting reactant at the catalyst surface, g mol/m^3
D_e	Effective diffusivity of limiting reactant in the catalyst pores, m^2/s
E_{act}/RT	Arrhenius group (activation energy, universal gas constant, temperature)
ΔH	Change in enthalpy of forward reaction (=283 KJ/g mol for CO oxidation)
k_p	Catalyst thermal conductivity, W/(m · K)
$Pe_{particle}$	Peclet number with particle diameter as characteristic length, dimensionless
Pe_r	Peclet number with reactor length in flow direction as characteristic length
R_{rxn}	Effective reaction rate, mol/(m^3 · s)
r_p	Catalyst particle radius, m
sccm	Volumetric gas flow referenced to 273.15 K and 1 atmosphere pressure, cm^3/min
T_s	Catalyst surface temperature taken as the bulk fluid temperature, K

ACKNOWLEDGMENTS

REFERENCES

1. Senkan, S., *Angew. Chem. Int. Ed.* **40**, 312 (2001).
2. Jandeleit, B., Schaefer, D. J., Powers, T. S., Turner, H. W., and Weinberg, W. H., *Angew. Chem. Int. Ed.* **38**, 2494 (1999).
3. Cong, P., Doolen, R. D., Fan, Q., Giaquinta, D. M., Guan, S., McFarland, E. W., Poojary, D. M., Self, K., Turner, H. W., and Weinberg, W. H., *Angew. Chem. Int. Ed.* **38**, 483 (1999).
4. Moates, F. C., Somani, M., Annamalai, J., Richardson, J. T., Luss, D., and Willson, R. C., *Ind. Eng. Chem. Res.* **35**, 4801 (1996).
5. Orschel, M., Klein, J., Schmidt, H. W., and Maier, W. F., *Angew. Chem. Int. Ed.* **38**, 2791 (1999).
6. Claus, P., Hönicke, D., and Zech, T., *Catal. Today* **67**, 319 (2001).
7. Senkan, S., Krantz, K., Ozturk, S., Zengin, V., and Onal, I., *Angew. Chem. Int. Ed.* **38**, 2794 (1999).
8. Pérez-Ramírez, J., Berger, R. J., Mul, G., Kapteijn, F., and Moulijn, J. A., *Catal. Today* **60**, 93 (2000).
9. Jensen, K. F., *Chem. Eng. Sci.* **56**, 293 (2001).
10. Ramsey, J. M., and Van den Berg, A., Eds. "Micro Total Analysis Systems 2001." Kluwer Academic, Boston, 2001.
11. Quiram, D. J., Ryley, J. F., Ashmead, J. W., Bryson, R. D., Kraus, D. J., Mills, P. L., Mitchell, R. E., Wetzel, M. D., Schmidt, M. A., and Jensen, K. F., *in* "Micro Total Analysis Systems 2001" (J. M. Ramsey and A. Van Den Berg, Eds.), p. 661. Kluwer Academic, Dordrecht, 2001.
12. Losey, M. W., Schmidt, M. A., and Jensen, K. F., *Ind. Eng. Chem. Res.* **40**, 2555 (2001).
13. Ajmera, S. K., Losey, M. W., Jensen, K. F., and Schmidt, M. A., *AIChE J.* **47**, 1639 (2001).
14. Wise, K. D., Ed. *Proc. IEEE* **86**, No. 8 (1998).
15. Senturia, S. D., "Microsystem Design," p. 3. Kluwer Academic, Boston, 2001.
16. Ayon, A. A., Braff, R., Lin, C. C., Sawin, H. H., and Schmidt, M. A., *J. Electrochem. Soc.* **146**, 339 (1999).
17. Schmidt, M. A., *Proc. IEEE* **86**, 1575 (1998).
18. Paul, B. K., Dewey, T., Alman, D., and Wilson, R., *in* "IMRET 4: 4th International Conference on Microreactor Technology, AIChE Spring National Meeting, Atlanta, 2000," p. 236. AIChE, 2000.
19. Knitter, R., Göhring, D., Bram, M., Mechnich, P., and Broucek, R., *in* "IMRET 4: 4th International Conference on Microreactor Technology, AIChE Spring National Meeting, Atlanta, 2000," p. 455. AIChE, 2000.
20. Martin, P. M., Matson, D. W., Bennett, W. D., Stewart, D. C., and Bonham, C. C., *in* "IMRET 4: 4th International Conference on Microreactor Technology, AIChE Spring National Meeting, Atlanta, 2000," p. 410. AIChE, 2000.
21. Bird, R. B., Stewart, W. E., and Lightfoot, E. N., "Transport Phenomena," pp. 84, 200, 559. Wiley, New York, 1960.
22. Sault, A. G., and Goodman, D. W., *Adv. Chem. Phys.* 153 (1989).
23. Ionnides, T., Efstathiou, A. M., Zhang, Z. L., and Verykois, X. E., *J. Catal.* **156**, 265 (1995).

24. Rainer, D. R., Koranne, M., Vesecky, S. M., and Goodman, D. W., *J. Phys. Chem. B* **101**, 10,769 (1997).
25. Oh, S. H., Fisher, G. B., Carpenter, J. E., and Goodman, D. W., *J. Catal.* **100**, 360 (1986).
26. Zafiris, G. S., and Gorte, R. J., *J. Catal.* **140**, 418 (1993).
27. Venderbosch, R. H., Prins, W., and Van Swaaij, W. P. M., *Chem. Eng. Sci.* **53**, 3355 (1998).
28. Oh, S. H., and Eickel, C. C., *J. Catal.* **128**, 526 (1991).
29. Levenspiel, O., "Chemical Reaction Engineering," p. 388. Wiley, New York, 1999.
30. Anderson, J. B., *Chem. Eng. Sci.* **18**, 147 (1963).
31. Rexwinkel, G., Heesink, A. B. M., and Van Swaaij, W. P. M., *Chem. Eng. Sci.* **52**, 3995 (1997).
32. Kunii, D., and Suzuki, M., *Int. J. Heat Mass Transfer* **10**, 845 (1967).
33. Tsai, P. K., Wu, M. G., and Maple, M. B., *J. Catal.* **127**, 512 (1991).